Journal of Structural Geology, Vol 13, No 7, pp 801 to 812, 1991
Printed in Great Britain

0191-8141/91 $03 00+0 00

Geometrical modeling of fault-related folds: a pseudo-three-dimensional approach

M. SCOTT WILKERSON

Department of Geology, University of Illinois, 245 NHB, 1301 W. Green St., Urbana, IL 61801, U.S.A.

DONALD A. MEDWEDEFF*

Department of Geological and Geophysical Sciences, Princeton University, Princeton, NJ 08544, U.S.A

and

STEPHEN MARSHAK

Department of Geology, University of Illinois, 245 NHB, 1301 W. Green St., Urbana, IL 61801, U.S.A.

(*Received* 20 *August* 1990; *accepted in revised form* 17 *January* 1991)

Abstract—Area-balanced cross-sections of ramp anticlines and tip-line folds in thin-skinned fold–thrust belts can be quantitatively constructed using plane-strain fault-bend and fault-propagation fold models. Cross-sections alone, however, are somewhat inadequate for interpreting along-strike changes in thrust-related fold geometry. Complex interplay between along-strike changes in fault slip and fault shape determines a range of geometric configurations which are difficult to visualize without the aid of quantitative three-dimensional models. We extend conventional two-dimensional folding theories into the third dimension by allowing for continuous variations in fault slip and fault shape along strike. Geometric equations relating map-view angles between fold axial-surface traces are derived for a case assuming a uniform fault geometry and an along-strike displacement gradient. The resulting folds possess no unique fold axis, but rather are characterized by multiple fold hingelines each corresponding to bends in the fault. For typical displacement gradients observed in the field, analysis of the models suggests that discernible differences exist between map patterns of fault-bend folds and fault-propagation folds, whereas little difference exists between map patterns of similar and parallel fault-bend folds. Map-view angles between axial-surface traces for parallel fault-bend folds and fault-propagation folds are a function of both ramp cutoff angle and fault slip, whereas these same angles for similar fault-bend folds are solely a manifestation of fault slip.

Examples assuming uniform shortening and continuously varying fault geometry along strike are also presented. Fault geometry is varied along strike to simulate oblique and lateral ramps. Depending upon model type and fault shape parameter modified, resulting folds exhibit either cylindrical or non-cylindrical fold geometries. Closure is generated by a decrease in fold amplitude where there is a decrease in ramp cutoff angle along strike or where a fault laterally cuts up section. In either instance, closure develops without varying shortening along strike. Model map patterns resemble actual thrust-related fold geometries and can be compared to maps of real structures to help predict subsurface geology.

INTRODUCTION

STRUCTURAL geologists long have relied on their artistic skills, geologic intuition and personal biases to depict fold–thrust belt geometries at depth. Cross-sections routinely are used to convey this information and are area balanced in the transport direction to strengthen the validity of the interpretation. An area-balanced cross-section is one that shows geologically reasonable structures for a given locale, and one that can be restored to an undeformed state such that the area of the cross-section in the undeformed state equals that in the deformed state (Dahlstrom 1969, 1970, Elliott 1983, Woodward *et al.* 1989). If plane strain is assumed, conservation of area in two dimensions represents conservation of volume in three dimensions.

Quantitative models of fold–thrust geometries and kinematics have been developed as tools for applying the balanced cross-section concept to cross-section interpretation (Suppe 1983, Suppe & Medwedeff 1984, Jamison 1987, Jones 1987, Mitra 1990, Suppe & Medwedeff in press). Present models simulate three distinct types of thrust-related folds characteristic of fold–thrust belts of which only two types will be addressed in this paper: fault-bend folds and fault-propagation folds. Fault-bend folds form in response to movement of strata over bends in a non-planar fault (Rich 1934, Suppe 1983), whereas fault-propagation folds develop by folding of strata immediately preceding a propagating tip line (Suppe & Medwedeff 1984, Suppe 1985). Two classes of fault-bend fold models commonly are used: the first assumes a similar fold geometry which

* Present address: ARCO Oil and Gas Company, 2300 W. Plano Parkway, Plano, TX 75075, U S.A.

allows strata to move past fault bends by shearing on imaginary vertical planes (vertical simple shear model; Sanderson 1982, Jones 1987, Wilkerson 1989b, 1990), whereas the other is a parallel-folding model (Sanderson 1982, Suppe 1983, Groshong & Usdansky 1988) in which strata deform by layer-parallel shear and axial surfaces bisect fold limbs The latter model yields area-balanced solutions only for cases in which the initial cutoff angle of a ramp connecting parallel upper and lower flats is less than 30°. Vertical simple shear is a likely model for rocks which behave isotropically with respect to mechanical layering, rocks which are vertically jointed, or rocks which are unlithified or unconsolidated. Layer-parallel shear is more likely in fault-related folds in which layering plays an important role in localizing strain (Apotria *et al.* in press). The fault-propagation fold model accommodates shortening by layer-parallel slip on bedding surfaces with fault slip decreasing to zero at the fault-tip line (Suppe & Medwedeff 1984, in press). This model is limited to ramp dips of less than 60°. All three models share properties that: (1) folds consist of panels of uniform dip separated by narrow hinge zones; (2) foot wall strata are undeformed; and (3) generated cross-sections are area balanced. The fundamental insight gained from these models is that fold geometry is principally a function of *fault geometry* and *fault slip*.

The purpose of our investigation is to extend these two-dimensional, kinematic models into the third dimension in order to study effects of continuous along-strike changes in fault slip (i.e. shortening) or fault shape (e.g. ramp height, cutoff angle and/or detachment level) on fold geometry. These models are considered *pseudo-three-dimensional* because they are created by linking a series of independent cross-sections along strike (cf. Snedden & Spang 1989, 1990 for a similar example). Linkage of sections along strike implicitly assumes deformation is restricted to planes parallel to each section (i.e. plane strain) and that strains in the strike direction are generally much smaller than in the transport direction, a reasonable assumption for non-metamorphic, thin-skinned, fold–thrust belts.

The assumption of plane strain is also, in part, justified by recent work by Apotria *et al.* (in press), who demonstrate that only minor out-of-plane deflection ($\leq 4.5°$ from the transport direction) occurs above oblique ramps for the ramp cutoff angles considered here; oblique ramps being the logical location for the maximum out-of-plane deflection for a given fault. Also, values of 10–20° out-of-plane deflections produce only minimal changes in area-balanced sections (Elliott 1976). We infer that our pseudo-three-dimensional models are a good first-order approximation to true three-dimensional geometries and kinematics.

Model map patterns are expeditiously constructed using forward-modeling computer software (Wilkerson 1989a, Wilkerson & Usdansky 1989) to link cross-sections sequentially along strike. These programs create: (1) volume-balanced block diagrams; (2) structure-contour maps of any stratigraphic unit; and/or (3) geologic maps of any horizontal erosion surface (Wilkerson 1989b, 1990) Structure-contour maps are an effective means of visualizing three-dimensional surfaces, and when combined with geologic maps, make for ready comparison of theoretical models with actual field examples. Synthetic generation of structure-contour and geologic maps also allows geologists to quickly and efficiently test multiple working hypotheses for a given fold with testable, reproducible models. No attempt is made in this paper to treat actual examples, however, as this work is still in progress.

Two types of along-strike variation are considered: models in which fault geometry is constant and displacement varies along strike and models in which displacement is constant and fault geometry varies along strike. The first case is explored in some detail by comparing map-view angles between axial-surface traces for the three models, both graphically and analytically, assuming a simple displacement gradient along strike (Wilkerson 1989b, 1990). Quantifying differences between fault-bend fold models is especially important because many commercial fault modeling programs (Gibbs 1983, Jones 1987, Wilkerson & Usdansky 1989) utilize the more versatile similar fault-bend fold model, thereby implicitly accepting limitations of its deformation mechanism by assuming that differences between folds produced by the similar fold model and those produced by the more commonly accepted parallel fold model are negligible. Quantitative comparison of the models provides a test for this assumption. The second case, due to the nearly infinite number of combinations, is only investigated graphically via analysis of computer-generated, structure-contour map patterns and volume-balanced block diagrams. Three types of changes in fault geometry are considered: change in fault dip, change in ramp height and change in detachment level. The first change simulates an oblique ramp, whereas the latter two model different forms of lateral ramps.

VARIABLE DISPLACEMENT MODELS

Similar and parallel fault-bend fold models

The kinematics for two-dimensional, parallel fault-bend fold evolution have been described previously (Suppe 1983, pp. 687–688, refer to his fig. 3). Briefly, kink bands A–A′ and B–B′ (Fig. 1) begin to grow in width and structural relief as slip occurs The distance between B and B′ along the fault is equal either to the displacement of the lowest cutoff or to the length of the fault ramp, whichever is less, whereas the distance between A and A′ is slightly less than the distance between B and B′ because slip is consumed by formation of the kink band. Axial surfaces A and B remain fixed with respect to the foot wall and hanging wall beds roll through these axial surfaces as slip proceeds. Axial surfaces A′ and B′ are fixed to the hanging wall beds and travel with the thrust sheet. This situation changes,

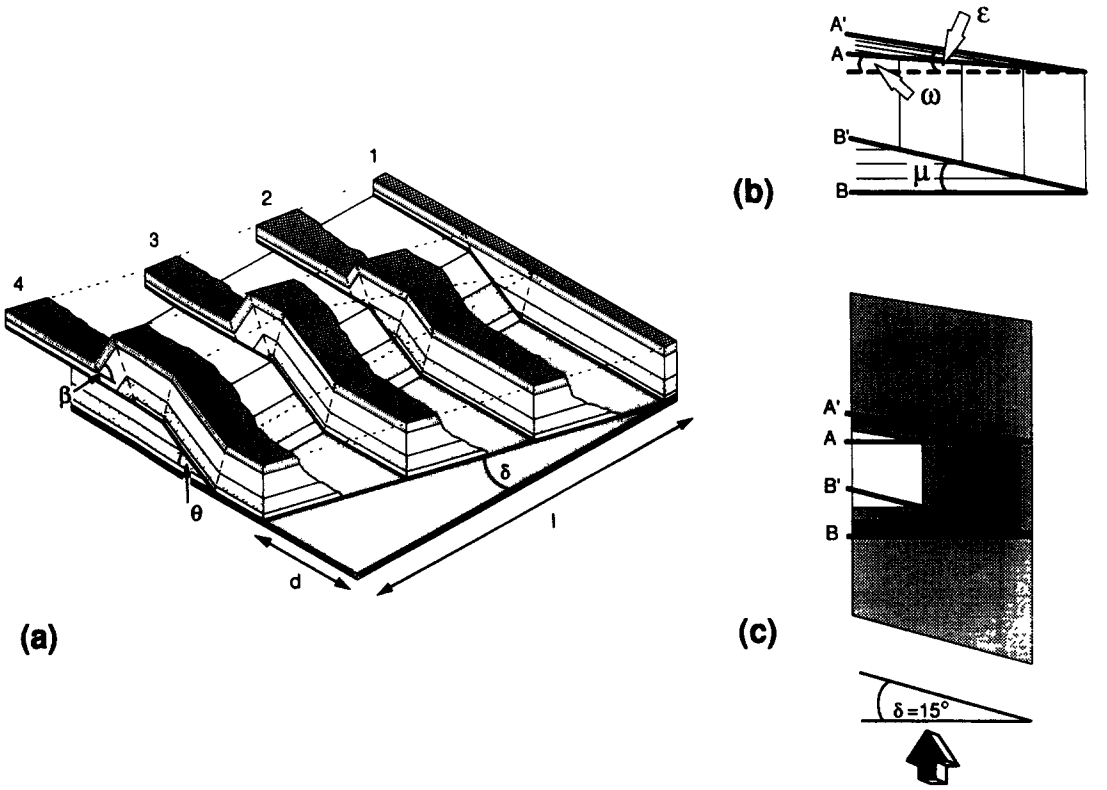

Fig. 1 (a) Cutaway block diagram depicting the three-dimensional fold geometry of a parallel fault-bend fold Fold parameters defined are: θ = ramp cutoff angle, β = forelimb angle, δ = displacement gradient (given as an angle), l = length along strike over which δ is maintained and d = shortening for a given cross-section at length l. Axial surfaces for the fold are: A′ = foreland syncline, A = foreland anticline, B′ = hinterland anticline and B = hinterland syncline (b) & (c) Map patterns of a parallel fault-bend fold with $\theta = 30°$ and $\delta = 15°$. These diagrams correspond to sections 1–3 in part (a). Arrow indicates sense of movement. (b) Structure-contour map of a layer above the upper flat. Map-view axial-surface angles of interest are: μ = angle between B and B′, ω = angle between a vertical plane parallel to the ramp strike and axial surface A, and ε = angle between a vertical plane parallel to the ramp strike and axial surface A′. (c) Horizontal geologic map of three layers above fault. Heavy lines indicate axial traces.

however, when axial surface B′ reaches the top of the fault ramp; B′ becomes pinned to the top of the ramp and the fold ceases to increase in structural relief. Axial surface A is released and the fold translates into the foreland without increasing kink-band width. Material continues to roll through axial surface B and B′, while axial surfaces A and A′ move passively with the hanging wall.

The kinematics for similar fault-bend folds (Fig. 2) are analogous to that for parallel fault-bend folds except (1) the width of kink bands A–A′ and B–B′ as measured in profile are both equal and (2) when axial surface B′ reaches the top of the ramp, axial surfaces B′ and A coincide; producing no intervening flat, before axial surface A migrates into the foreland along the upper flat. In other words, in parallel fault-bend folds, A and B′ never merge, whereas in similar fault-bend folds, A and B′ may coincide at the ramp crest. This relationship exists because axial surfaces bisect fold limbs for parallel fault-bend folds, whereas axial surfaces always remain vertical for similar fault-bend folds.

Figures 1(a) and 2(a) depict cutaway three-dimensional diagrams for parallel fault-bend and similar fault-bend fold terminations, respectively (Medwedeff 1985). These figures and all of the following derivations assume that the fault-bend fold geometry consists of parallel upper and lower flats separated by a single intervening ramp. Both figures possess a constant fault geometry and an along-strike displacement gradient of angle δ. Each fault-bend fold terminates into a non-cylindrical fold which consists of foreland and hinterland synclinal and anticlinal fold pairs (axial surfaces A–A′ and B–B′ in Figs. 1a and 2a) in which axial surfaces separate the overall structure into planar dip panels. The line of intersection of each axial surface with bedding defines a hingeline which marks the change in orientation between adjacent dip panels (Medwedeff 1985). Each hingeline changes orientation based upon changes in fault slip and fault geometry. Anticlinal axial surfaces (B′ and A) exhibit along-strike changes in orientation in regions either side of where axial surface B′ reaches the top of the ramp. Synclinal axial surfaces (A′ and B) are not as geometrically variable; the hinterland synclinal axial surface (B) always remains parallel to the ramp base, whereas the foreland synclinal axial surface (A′), being fixed to the stratigraphically highest hanging-wall cutoff line, is oblique to the fault ramp.

Equations defining angular relations between map traces of axial surfaces for similar and parallel fault-bend fold models are derived by extending two-dimensional equations for area-balanced cross-sections into the third dimension assuming a constant displacement gradient along strike (Wilkerson 1989b, 1990).

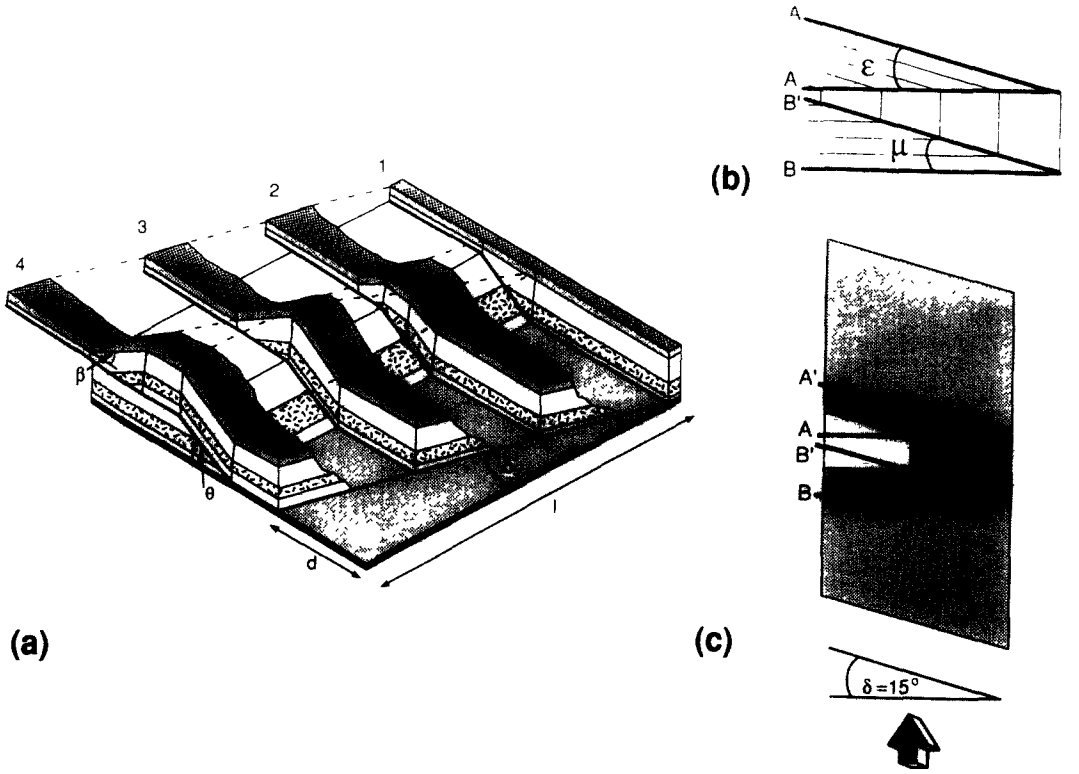

Fig 2. (a) Cutaway block diagram depicting the three-dimensional fold geometry of a similar fault-bend fold Fold parameters are defined in Fig. 1. (b) & (c) Map patterns for a similar fault-bend fold with $\theta = 30°$ and $\delta = 15°$ These diagrams correspond to sections 1–3 in part (a). Arrow indicates sense of movement. (b) Structure-contour map of a layer above the upper flat. (c) Horizontal geologic map of three layers above fault. Heavy lines indicate axial traces.

Geometric relationships derived from these equations provide a means for quantitatively comparing these models. Figures 1(b) and 2(b) are structure-contour maps for the respective fault-bend fold models. These maps represent only sections 1–3 on Figs. 1(a) and 2(a), respectively. Three angles (μ, ω and ε) allow the entire fold to be quantitatively described: μ is the angle between map traces of axial surfaces B and B′, ω is the angle between map traces of a vertical plane parallel to the strike of the ramp and axial surface A, and ε measures the angle between map traces of a vertical plane parallel to the strike of the ramp and axial surface A′ (Figs. 1b and 2b). In the following equations δ is displacement gradient, θ is ramp cutoff angle, l is length along strike over which δ is maintained, d is shortening for a given cross-section at a distance l and β is the forelimb angle. To find μ for parallel fault-bend folds:

$$\tan \delta = \frac{d}{l} \tag{1}$$

$$\tan \mu = \frac{x}{l}, \tag{2}$$

where x is map-view distance between B and B′ equal to $d \cos \theta$. Therefore,

$$\tan \mu = \cos \theta \tan \delta. \tag{3}$$

For similar fault-bend folds, each bed in the hanging wall is displaced horizontally by a constant heave and is subsequently vertically sheared. Therefore,

$$\tan \mu = \tan \delta. \tag{4}$$

To determine ω for parallel fault-bend folds, the structural relief of the fold must be known. The height of the anticline above the upper flat is $d \sin \theta$ up to a maximum value equal to the ramp height (based on Suppe 1983). If y is the map-view distance between A and the vertical plane parallel to the strike of the ramp, then the equation relating y with fold relief is:

$$y = \tan \frac{\beta}{2} d \sin \theta \tag{5}$$

and

$$\tan \omega = \frac{y}{l}. \tag{6}$$

Substituting equations (1) and (5) into equation (6) yields:

$$\tan \omega = \sin \theta \tan \delta \tan \frac{\beta}{2}. \tag{7}$$

Similar fault-bend folds, by definition, possess vertical axial surfaces, and thus axial surface A and the map trace of a plane parallel to the strike of the ramp are parallel. Therefore,

$$\tan \omega = 0. \tag{8}$$

To find ε for parallel fault-bend folds, the distance between a vertical plane parallel to the strike of the

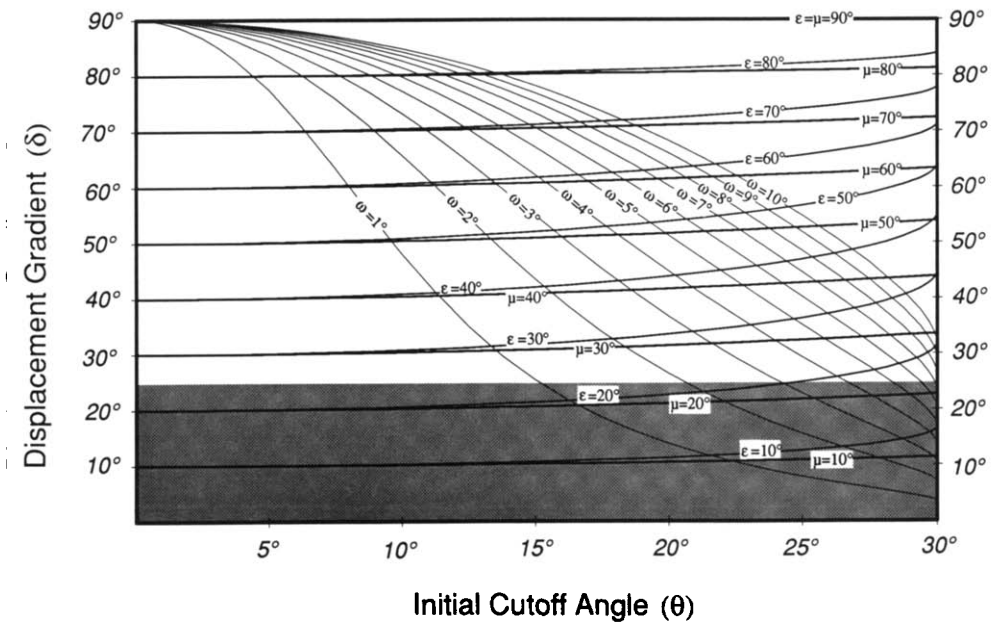

Fig. 3. Graph of relationship between initial cutoff angle θ, displacement gradient δ, and map-view angles between axial surfaces μ, ω and ε for parallel fault-bend folds; based on equations (4), (7) and (9). Shaded area indicates values commonly observed in nature.

ramp at the ramp crest and A′ is $(d \sin \theta)/\sin \beta$ (based on Suppe 1983). Therefore,

$$\tan \varepsilon = \frac{\frac{d \sin \theta}{\sin \beta}}{l} = \frac{\sin \theta \tan \delta}{\sin \beta}. \quad (9)$$

For similar fault-bend folds, again due to constant heave throughout the hanging wall, the equation for ε is

$$\tan \varepsilon = \tan \delta. \quad (10)$$

Figure 3, a graph constructed from equations (3), (7) and (9) for parallel fault-bend folds, permits quick visual assessment of the possible range of solutions for a given situation. For example, a fault with a constant dip of 25° and a displacement gradient of 20° possesses axial-surface angles for μ, ω and ε of 18°, 2.6° and 16°, respectively. Conversely, if measurements of $\mu = 13°$, $\omega = 2.8°$ and $\varepsilon = 11°$ are consistent for a given distance along strike, a good estimate for ramp dip and displacement gradient over that interval is 28° and 15°, respectively. In general, any combination of two knowns are sufficient to solve for the remaining three unknowns. A graph for similar fault-bend folds would be a series of straight lines with $\mu = \varepsilon = \delta$ (displacement gradient) and $\omega = 0$ and is not provided. The preceding equations coupled with Fig. 3 demonstrate that angles between axial traces in similar fault-bend folds are solely the manifestation of the displacement gradient, whereas angles between axial traces for parallel fault-bend folds are a function of both ramp dip and displacement gradient. Ramp dip and fault slip are also the controlling factors for the respective two-dimensional models.

Although the complete range of displacement gradients is shown in Fig. 3, natural continuous displacement gradients under non-metamorphic conditions are probably small. Measurements of displacement gradients for natural structures include 10–25° for major thrusts in the Canadian Rocky Mountains (Elliott 1976, Fermor 1990), 6–25° for the Pine Mountain thrust (Mitra 1988), and 15° at Wheeler Ridge anticline in southern California (Medwedeff in press). Assuming 25° as an upper limit, angles between axial traces for parallel fault-bend folds typically range 0–25° for μ, 0–7° for ω, and 0–25° for ε (Fig. 3, shaded region). μ for similar fault-bend folds ranges between 0° and 25°, whereas ω is 0° and ε is between 0° and 25°.

Figure 4 provides a quantitative comparison between the similar and parallel fault-bend fold models by plotting angular differences between angles μ and ε for displacement gradients up to 90° and ramp cutoff angles up to 30°. Assuming a maximum displacement gradient of 25°, the models are almost indistinguishable based upon axial-surface relationships alone (Fig. 4, left of dashed lines). The largest differences in axial-surface relationships exist in the forelimb of the folds (Fig. 4b), yet these too, are insignificant at displacement gradients less than 25°.

Although quantitatively insignificant and easily within the error of measurement in the field, these slight forelimb differences may be qualitatively observed, even for small displacement gradients, on synthetic structure-contour maps and geologic maps for similar and parallel fault-bend fold terminations (Figs. 1b & c and 2b & c). Figures 1(b) and 2(b) are structure-contour maps of an unfaulted layer above the upper flat of the fault. The structure-contour maps illustrate the axial-surface relationships previously discussed as well as display the non-parallel nature of the fold termination hingelines. Figures 1(c) and 2(c) are horizontal sections of the models which approximate geologic maps of folds exposed by erosion. These synthetic maps are constructed for the same boundary conditions as the

structure-contour maps in Figs. 1(b) and 2(b), respectively For similar fault-bend folds, axial-surface relationships depicted on the geologic map (Fig. 2c) are the same as those depicted on the structure-contour map in Fig 2(b), whereas for parallel fault-bend folds, axial relationships shown on the geologic map (Fig 1c) are different than those depicted on the structure-contour map in Fig. 1(b). Specifically, the geologic map lacks an angle ω (Fig 1c), a difference which occurs because the parallel fault-bend fold has inclined axial surfaces. Angles measured on structure-contour maps reflect the three-dimensional orientations of axial surfaces, whereas geologic maps display an apparent angle of the axial-surface trace at the specified erosion level. Similar fault-bend folds possess vertical axial surfaces and are not affected by the apparent angle. Clearly, the type of map used to describe a fault-bend fold is important for accurate interpretation of the fold axial-surface relationships

Distinguishing between similar and parallel fault-bend folds in the field is tenuous at best. Our previous discussion points to the potential utility of using synthetic axial-surface relationships to distinguish between the two models. Specifically, the presence of ω is diagnostic for parallel fault-bend folds. In practice, the resolution of actual structure-contour maps for single ramp anticlines may not be sufficient to select the appropriate model. In such cases, the geologist must rely upon bed thicknesses, axial-surface orientations

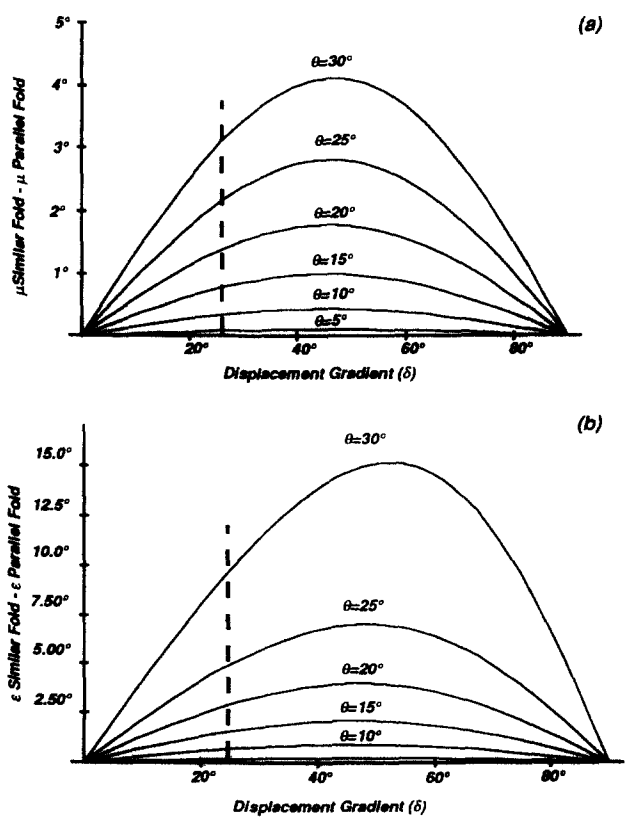

Fig 4 Comparison of μ and ε for parallel and similar fault-bend folds with constant fault geometry and variable displacement gradient Values left of dashed line are commonly observed in nature (a) Differences in μ (b) Differences in ε

with respect to bedding, or strain patterns indicative of the mode of deformation to determine the appropriate model Should the information be non-unique, using either model would not induce serious error for fault-related folds with a small ramp cutoff angle.

Fault-propagation fold model

Figure 5(a) depicts a cutaway three-dimensional diagram for a parallel fault-propagation fold termination (Medwedeff 1985). Like both fault-bend fold model terminations, the fault-propagation fold model assumes plane strain, constant fault geometry, and a constant displacement gradient along strike. The fault-propagation fold model, however, is distinct from either fault-bend fold model because as the fault propagates from the lower décollement, beds are successively folded and then faulted as slip on the fault increases. This results in a single anticlinal axial surface (C) for the faulted layers which bifurcates to form axial surfaces B′ and A for unfaulted layers (Fig. 5a).

The fault-propagation fold termination consists of multiple non-parallel hingelines defined by the intersection of bedding and the axial surfaces. The orientation of each hingeline is related to changes in the ramp cutoff angle and fault slip. Axial surface B parallels the ramp and axial surfaces A′ and B′ are oblique to the ramp with B′ plunging in the direction of decreasing displacement. Axial surface A exhibits a variety of possible geometries depending on the ramp cutoff angle (Figs. 5b and 6). Axial surfaces A and B′ join along a plunging line to form a single axial surface C. The line of bifurcation of axial surface C is located at the same stratigraphic level as the displacement-controlled fault tip and is in a different stratigraphic horizon in each section.

Geometric analysis of a fault-propagation fold termination uses the same fold parameters used to describe fault-bend folds (Fig. 5b). For a given stratigraphic layer, a constant along-strike fault geometry, and an along-strike displacement gradient, unique sections exist along strike which contain no displacement and a point of bifurcation (intersection of axial surfaces A and B′) for that layer, respectively (Fig. 7; C and D are on the undeformed section and C′ and D′ are both in the section containing the point of bifurcation). All angular relationships are determined only for the region between these sections. μ is the angle between map traces of axial surfaces B′ and B (Fig. 5b). The map-view distance between B and B′, x, for the section containing the point of bifurcation is:

$$x = \left[d\left(1 + \frac{h}{r}\right) \right] \cos\theta, \qquad (11)$$

where h is any arbitrary bed height and r is ramp height as measured from the basal detachment (based on Suppe & Medwedeff 1984, in press, Suppe 1985). Substituting equations (11) and (1) into equation (2) produces·

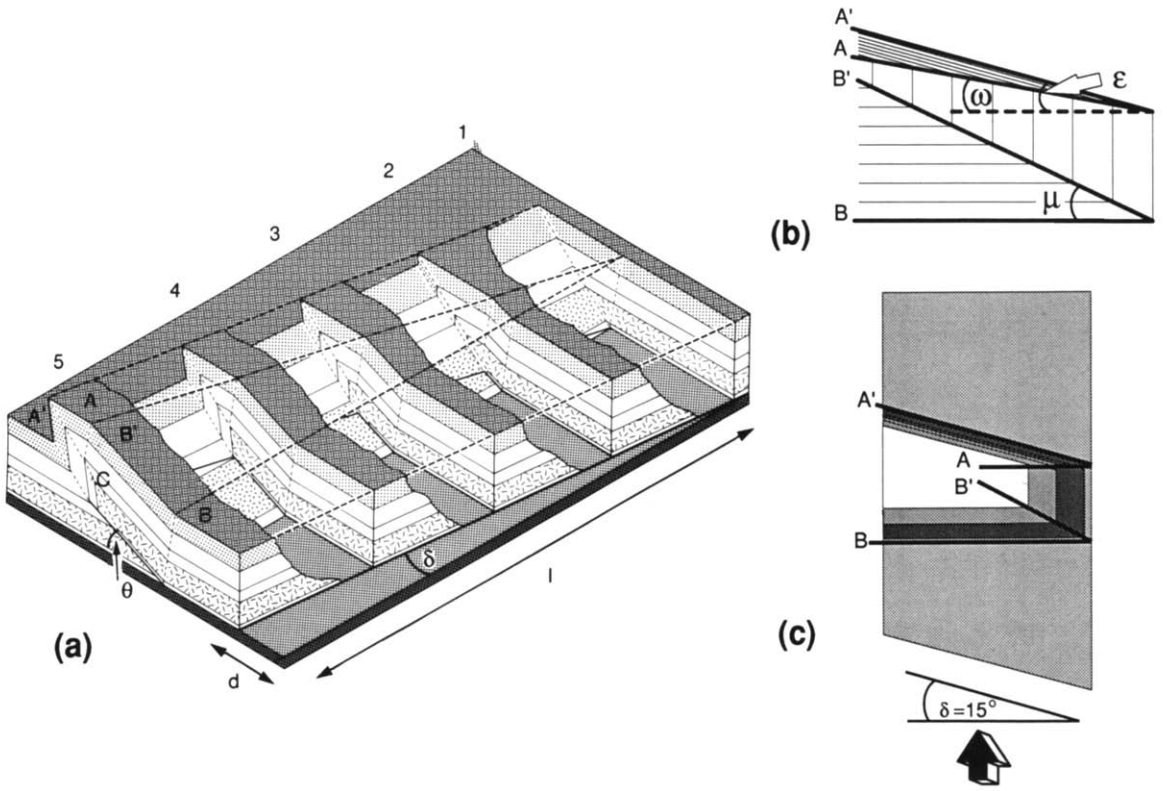

Fig. 5. (a) Cutaway block diagram depicting the three-dimensional fold geometry of a fault-propagation fold. Fold parameters are defined in Fig. 1. (b) & (c) Map patterns for a fault-propagation fold with $\theta = 30°$ and $\delta = 15°$. Arrow indicates sense of movement. (b) Structure-contour map of an unfaulted layer. (c) Horizontal geologic map of three layers above fault. Heavy lines indicate axial traces.

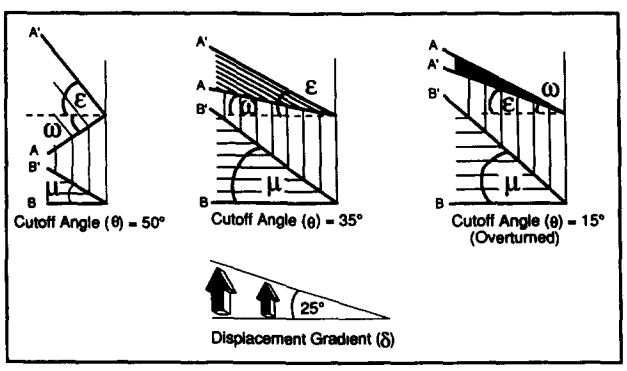

Fig 6. Structure-contour maps for fault-propagation folds illustrating fold geometry as a function of ramp cutoff angle. Ramp cutoff angles decrease from left to right. δ is 25°.

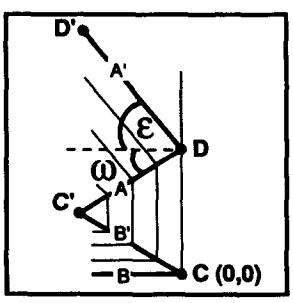

Fig. 7. Structure-contour map depicting co-ordinate system used for determining angular relations between axial surfaces for fault-propagation folds. Points C and D are on the undeformed cross-section and points C′ and D′ are in the section containing the point of bifurcation. Point C is given co-ordinates (0, 0). Co-ordinates of other points are determined based on equations provided in the text and on equations in (Suppe & Medwedeff 1984, in press, Suppe 1985). Angles ω and ε are found by calculating the slopes of axial traces C′D (A) and D′D (A′) and subtracting the values from 90°, respectively.

$$\tan\mu = \left[1 + \frac{h}{r}\right]\cos\theta\tan\delta. \tag{12}$$

For $h = 0$, this equation is equivalent to equation (3) for parallel fault-bend folds. For $h \geq r$, the equation is always

$$\tan\mu = 2\cos\theta\tan\delta. \tag{13}$$

The angles ω and ε are determined by first finding the slope of axial traces D–C′ and D–D′ (Fig. 7), respectively, and then by subtracting these angles from 90°. Two points defining the slope of axial trace D–C′ are the point of bifurcation (C′) and the point where axial surface A intersects the undeformed section (D). If point C has co-ordinates (0, 0), co-ordinates for C′ are (2 cos θ tan δ, d/tan δ). Given any arbitrary bed height h, co-ordinates for D are (h(tan β/2 + tan θ/2), 0). The bed height at the point where the anticlinal axial surface bifurcates is equivalent to the ramp height and is defined by:

$$h = r = \frac{2d\sin(\beta + \theta)\sin\theta}{\sin\beta} \tag{14}$$

(based on Suppe & Medwedeff 1984, in press, Suppe 1985). Substituting equation (14) into the slope calculation produces:

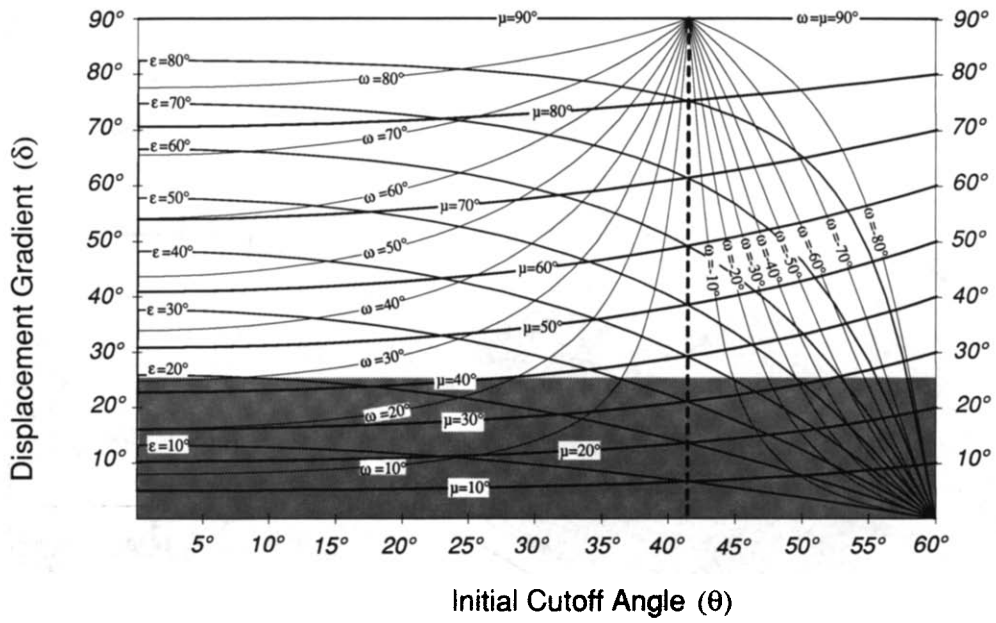

Fig. 8. Graph of relationships between initial cutoff angle θ, displacement gradient δ, and map-view angles between axial surfaces μ, ω and ε for fault-propagation folds; based on equations (13), (15) and (16). Shaded area indicates values commonly observed in nature. Dashed line separates regions of positive and negative ω.

$$\omega = 90 - \arctan \times \left[\frac{\sin\beta}{2\tan\delta[\cos\theta\sin\beta - \sin(\beta+\theta) \times \sin\theta[\tan(\beta/2) + \tan(\theta/2)]]} \right]. \quad (15)$$

Similarly, ε is found to be:

$$\varepsilon = 90 - \arctan \times \left[\frac{\sin\beta}{2\tan\delta\sin(\beta+\theta) \times [1 - \sin\theta[\tan(\beta/2) + \tan(\theta/2)]]} \right]. \quad (16)$$

Figure 8 illustrates the range of solutions defined by equations (13), (15) and (16) for a given ramp cutoff angle and displacement gradient. Again, discounting values for displacement gradients greater than 25°, typical ranges for μ, ω and ε are 0–45°, −89–31° and 0–80°, respectively (Fig. 8, shaded region). Further inspection of Fig. 8 indicates that for a given displacement gradient, increasing the cutoff angle produces a corresponding augmentation in ε which increases rapidly for cutoff angles exceeding 45°. Similarly, increasing the cutoff angle causes axial surface A to migrate toward the hinterland (See Fig. 6), producing a reduction in ω. As θ increases beyond 41.4° (dashed line, Fig. 8), ω becomes increasingly negative in our co-ordinate system. This change in ω is illustrated in Fig. 6.

Comparison of fault-bend and fault-propagation fold models

Because both fault-propagation and parallel fault-bend folds deform by layer-parallel shear and because both their geometries are a function of fault geometry and fault slip, comparison of these fold types is a natural next step in analyzing thrust-related fold terminations. Equations (3) and (13) establish that for $h \geq r$

$$\tan\mu_{\text{fault-propagation fold}} = 2\tan\mu_{\text{parallel fault-bend fold}}. \quad (17)$$

μ is always larger in fault-propagation folds for a given cutoff angle and displacement gradient than in fault-bend folds with the same parameters, but is not twice as large as might be inferred from casual inspection of equations (3) and (13). Based on analytical solutions plotted in Figs. 3 and 8, differences in μ between parallel fault-bend and fault-propagation folds reach a magnitude of nearly 20°. Differences of such magnitude are significant and could be measured in the field. Inspection of plots for ε (Figs. 3 and 8) reveals that for cutoff angles less than ≈21.5°, parallel fault-bend folds have larger ε values than fault-propagation folds. Conversely, fault-propagation folds possess larger ε values for angles larger than ≈21.5°, a relationship which occurs because the fault-propagation fold is overturned with a steeply dipping forelimb at low cutoff angles and becomes progressively more open as the cutoff angle increases (Fig. 6). Distinct differences in magnitude and orientation of ω also distinguish the two fold types. Fault-propagation folds are characterized by a wide range of orientations and magnitudes of ω as compared with fault-bend folds (Figs. 3 and 8), and, unlike fault-bend folds, may possess negative ωs for high cutoff angles and ωs larger than ε for faults with low cutoff angles and overturned beds (Fig. 6). For intermediate cutoff angles, fault-propagation folds resemble fault-bend folds, but have a much larger μ (Fig. 6). Our results suggest that fault-propagation folds should be distinguishable from fault-bend folds based on map patterns and axial-surface relationships.

VARIABLE FAULT GEOMETRY MODELS

Investigation of along-strike changes in fault geometry with constant along-strike shortening provides

insight into the contribution of fault shape to three-dimensional changes in thrust-related fold geometry. We limit our analysis to studying effects of along-strike changes in ramp cutoff angle, basal detachment level and ramp height on fold geometry for each fold type. These three cases simulate oblique ramps, entire faults cutting up section from the basal décollement, and lateral ramps cutting up section from the upper detachment, respectively. Shortening is held constant for all models. For fault-propagation folds, ramp height and shortening are not independent parameters (Suppe & Medwedeff in press); changes in ramp cutoff angle produce variable ramp heights if constant shortening is maintained. Therefore, because shortening is held constant in our analysis, the case involving changing the ramp height for fault-propagation folds is omitted.

Oblique fault ramps are fault ramps which are neither perpendicular nor parallel to the transport direction of the hanging wall. We simulate oblique fault ramps by varying ramp cutoff angle along strike (Fig. 9), a situation not uncommon in nature (e.g. House & Gray 1982, Fischer & Woodward 1990). In Fig. 9, ramp cutoff angles decrease progressively along strike from 30° to 15° for all three fold types (30° was chosen due to limitations imposed by the parallel fault-bend fold model). The cutoff angles are measured in the direction of transport and effectively serve as apparent cutoff angles for a true oblique ramp. Shortening, ramp height (except for fault-propagation folds) and basal ramp location are held constant. The backlimb contours for all fold types do not remain parallel to the lower ramp hinge, but curve, as do contours in the forelimb, toward the foreland as the cutoff angle decreases (Fig. 9). Because ramp height and shortening are held constant for the fault-bend fold models, decreasing the ramp dip creates a longer fault ramp, thus resulting in a foreland migration of the upper ramp hinge (Figs. 9a & b). Decreasing ramp dip for fault-bend models also causes a decrease in fold amplitude and an increase in map-view separation of axial-surface traces. The decrease in fold amplitude results in a structure-contour map pattern resembling that for a decrease in fault slip along strike (compare Figs. 9a & b with Figs. 1b and 2b). The increase in map-view separation for fault-bend folds is observed in both the forelimb and backlimb and is given in the backlimb by

$$s = d \cos \theta, \tag{18}$$

where s is map-view separation of axial-surface traces B–B′, d is shortening and θ is the ramp cutoff angle. This relationship suggests as θ decreases, s increases, a proposal that is supported by structure-contour maps of fault-bend folds (Figs. 9a & b). The two fault-bend fold models produce very similar structures, as expected from our previous arguments.

Decreasing the ramp cutoff angle for fault-propagation folds also generates a fold termination which resembles a termination created by decreasing displacement along strike (compare Fig. 9c with Fig. 5b). Maintaining constant shortening and decreasing the ramp cutoff angle causes a corresponding decrease in the ramp height and fold amplitude (Fig. 9c; confirmed by equation 14), which results in a hinterland migration of the ramp for a given amount of shortening. In addition, decreasing the ramp cutoff angle for a fault-propagation fold requires that the fold becomes overturned. House & Gray (1982) observed similar relationships in the field. Moreover, our analysis suggests that a fault-propagation fold termination with closure in the opposite direction can also be formed by steepening ramp dip along strike while holding ramp height constant, a change which automatically produces a decrease in shortening.

The last two variations in fault geometry to be investigated are changes in detachment level along strike, both of the upper and lower detachments (Figs. 10 and 11). A change in detachment level results in a lateral ramp cutting up section in the direction of the higher detachment. Lateral ramps are common in nature and may cause significant changes in fold geometry (Dahlstrom 1970, Harris & Milici 1977, Mitra 1988). For these model examples, shortening and ramp cutoff angle (30°) are held constant for all fold types and detachments cut up section at an arbitrary angle of 26.6°. Analysis of the resulting fold is facilitated by tracing the fate of a horizontal layer at a given height, which is unfaulted for lower detachments, but eventually becomes truncated as the fault cuts up section.

For the first type of lateral ramp considered, the

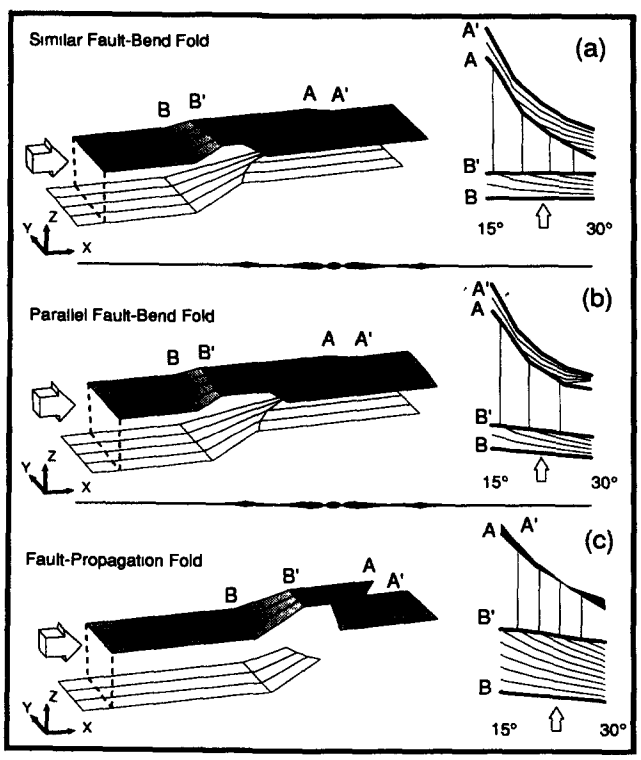

Fig. 9. Diagrams depicting pseudo-three-dimensional fold geometry due to an oblique ramp Ramp angles vary from 30° (nearest) to 15° (farthest). Corresponding structure-contour map of a layer above the fault right of each block diagram. Arrows indicate sense of movement. (a) Similar fault-bend fold, (b) parallel fault-bend fold and (c) fault-propagation fold.

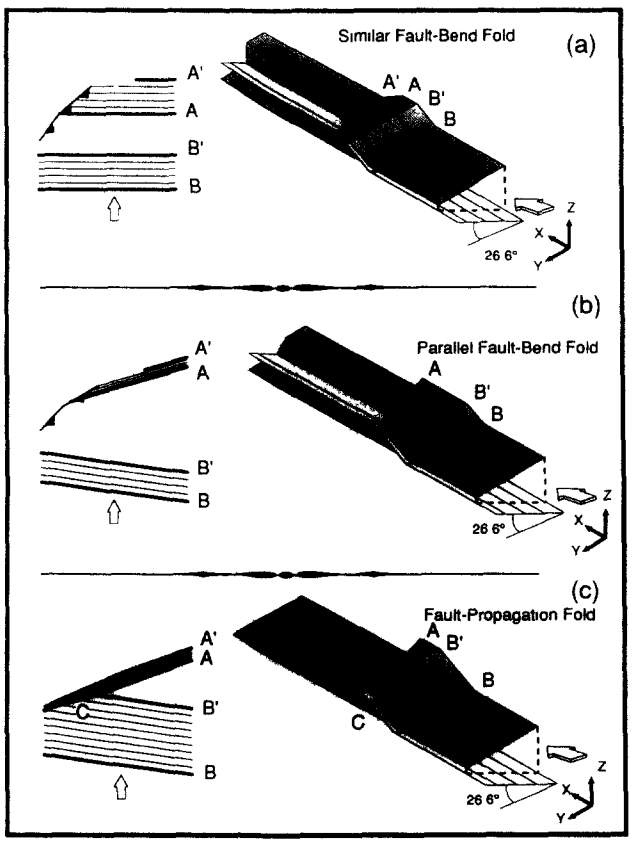

Fig. 10 Diagrams depicting pseudo-three-dimensional fold geometry due to a fault cutting up section from a basal décollement The ramp height and ramp angle (30°) are held constant. Corresponding structure-contour map of a layer truncated by the fault left of each block diagram Arrows indicate sense of movement. (a) Similar fault-bend fold, (b) parallel fault-bend fold and (c) fault-propagation fold

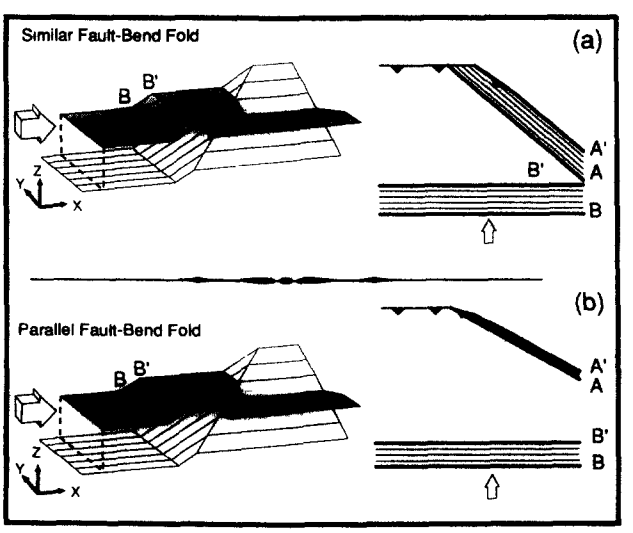

Fig 11 Diagrams depicting pseudo-three-dimensional fold geometry due to an upper décollement cutting up section. The ramp angle is held constant at 30° Corresponding structure-contour map of a layer truncated by the fault right of each block diagram. Arrows indicate sense of movement. (a) Similar fault-bend fold and (b) parallel fault-bend fold

entire fault laterally cuts up section from the basal décollement The parallel fault-bend fold possesses converging axial traces with forelimb and backlimb contours not parallel to the ramp base, whereas the similar fault-bend fold is cylindrical with contours parallel to the ramp base (Figs. 10a & b). This contrast in styles arises because as the the fault cuts up section along strike any particular bed intersects axial surfaces at lower positions Because similar fault-bend folds possess vertical axial surfaces, the structure is not altered by lateral ramping, whereas parallel fault-bend folds have inclined axial surfaces whose intersection produces a conical-like fold. In contrast to the oblique ramp case, spacing of contours in both the forelimb and backlimb are constant for folds produced by both models. Eventually each layer is completely truncated and becomes part of the foot wall. The fault-propagation fold model produces a geometry similar to the parallel fault-bend fold model (Figs. 10b & c). The fold axial traces converge and structure contours of the layer are not parallel to the ramp base. The fault-propagation fold can be distinguished from the parallel fault-bend fold, however, by the fault orientation with respect to the fold and by the closure of the structure contours. The structure contours for the fault-propagation fold indicate a very tight anticline that is truncated by the fault at a low angle, whereas the parallel fault-bend fold produces a more open anticline with an abrupt truncation of contours by the fault (Figs. 10b & c)

The last case investigated is the upper detachment of fault-bend folds cutting up section (Fig. 11). A fault-propagation fold model was not generated for this case because we chose to restrict our study to constant shortening examples in order to investigate the contribution of variation of fault geometry to thrust-related fold terminations. Changing ramp heights would have resulted in corresponding changes in shortening. Comparison of the structures produced by the similar and parallel fault-bend fold models indicates the main difference between the two fold types is that the former produces a tighter anticline. Both folds possess convergent fold axes with backlimb contours parallel to the ramp base and forelimb contours oblique to the ramp base. Closure of the folds is opposite in sense to the direction in which the upper detachment cuts up section. The closure of contours is also opposite in direction to the case of the entire fault cutting laterally up section from a basal décollement.

In summary, abrupt changes in fold geometry are inferred to originate not only as a consequence of decrease in fault slip along strike, but also in response to lateral ramps cutting up-section and to ramp cutoff angle changes along strike. Undoubtedly, natural fold terminations result from complex combinations of all three factors. These models suggest means by which cylindrical and some types of non-cylindrical thrust-related fold terminations can form. Careful comparison of computer-generated map patterns with well-constrained, field examples might suggest what types of

along-strike changes are occurring in fault slip, fault shape and folding style.

DISCUSSION AND CONCLUSIONS

Fault geometry and fault slip clearly exert a fundamental control on both two- and three-dimensional fault-related fold geometry. Where fault geometry is constant and fault slip varies along strike, significant differences in three-dimensional geometries and structural-contour map patterns exist between fault-bend folds and fault-propagation folds. In contrast, similar and parallel fault-bend folds are nearly indistinguishable for typical ramp angles and displacement gradients. Angles between axial traces for similar fault-bend folds are a manifestation of only the displacement gradient, whereas angles between axial traces for parallel fault-bend and fault-propagation folds are a function of both the displacement gradient and ramp cutoff angle. The lateral terminations of these thrust-related folds do not yield a unique fold axis, but rather consist of multiple fold hingelines separating dip domains, each corresponding to bends in the fault. The fold terminations are neither cylindrical nor conical, but are more aptly described as non-cylindrical structures consisting of several nonparallel hingelines.

Changes in fault shape also exert substantial control on the geometry of thrust-related fold terminations. The resulting folds can be cylindrical or non-cylindrical and can exhibit different directions of closure depending on the model type and the fault shape parameter modified. Closure of a thrust-related fold is generated by a decrease in fold amplitude due to a smaller ramp cutoff angle or to a fault cutting up-section laterally. In either case, no decrease in shortening is necessary in order to obtain closure.

Through the use of psuedo-three-dimensional models, we have described qualitative and quantitative criteria for distinguishing between three commonly used thrust-related fold models under various conditions of fault slip and fault geometry. We suggest that analysis of angular relationships between axial surfaces of thrust-related fold terminations provides a meaningful way of interpreting the subsurface geometry of the fold and suggests possible alternatives for describing the interplay between along-strike changes in fault slip, fault shape and folding style. The pseudo-three-dimensional models presented in this paper are intended to provide representative end-members with precise geometries and kinematics against which relevant field examples may be considered. They are not intended to represent any specific fold, nor precisely describe actual three-dimensional strain mechanisms. These models are best used as plane-strain standards by which the amount of out-of-plane strain and the position material points deviate from plane strain to non-plane strain displacement path trajectories can be determined. Elliott (1976) estimates that 10–20° of out-of-plane strain produces minimal changes to area-balanced sections. We infer that our pseudo-dimensional models approximate natural geometries under similar conditions.

Acknowledgements—This material is based, in part, upon work by M S Wilkerson supported by a National Science Foundation Fellowship Support of D A. Medwedeff at Princeton University was provided by the Department of Geological and Geophysical Sciences, ARCO Oil and Gas, and Texaco U.S.A Travel funds for M. S Wilkerson to present aspects of this work was provided by the Department of Geology and the Graduate College at the University of Illinois. This paper benefitted from constructive comments and discussions with Istvan Barany, William Bosworth, Mark Fischer, Chris Hedlund and George de Vries Klein, and from the reviews of Ted Apotria and an anonymous reviewer for which they are all gratefully acknowledged. A portion of the drafting was provided by ARCO Oil and Gas Company and the Department of Geology at the University of Illinois in the person of Jessie Knox

REFERENCES

Apotria, T. G., Snedden, W T., Spang, J H & Wiltschko, D. V. In press. Kinematic models of deformation at an oblique ramp. In: *Thrust Tectonics* (edited by McClay, K. R.). Unwin-Hyman Press, Arnhem, The Netherlands

Dahlstrom, C. D. A 1969. Balanced cross-sections. *Can. J. Earth Sci.* **6**, 743–757.

Dahlstrom, C. D. A. 1970. Structural geology in the eastern margin of the Canadian Rocky Mountains. *Bull. Can Petrol Geol* **18**, 332–406.

Elliott, D. 1976. The energy balance and deformation mechanisms of thrust sheets. *Phil. Trans. R. Soc.* **A283**, 289–312

Elliott, D. 1983. The construction of balanced cross-sections *J. Struct Geol.* **5**, 101.

Fermor, P. R. 1990. Aspects of the three-dimensional geometry of thrust sheets in the Alberta foothills 1990 *Thrust Tectonics Conf. Abs.* 32.

Fischer, M. P & Woodward, N. B. 1990. Non-Eulerian thrust systems in Tennessee and Idaho–Wyoming 1990 *Thrust Tectonics Conf. Abs.* 72.

Gibbs, A. 1983. Balanced cross section construction from seismic sections in the areas of extensional tectonics *J. Struct. Geol.* **5**, 153–160.

Groshong, R. H. & Usdansky, S. I. 1988 Kinematic models of plane-roofed duplex styles. In: *Geometries and Mechanisms of Thrusting* (edited by Mitra, G. & Wojtal, S.). *Spec Pap geol. Soc. Am.* **222**, 197–206.

Harris, L. D. & Milici, R C 1977 Characteristics of thin-skinned style of deformation in the southern Appalachians and potential hydrocarbon traps. *Prof. Pap. U S geol. Surv.* **1018**

House, W M. & Gray, D. R. 1982. Displacement transfer at thrust terminations in Southern Appalachians-Saltville thrust as example *Bull. Am. Ass. Petrol. Geol.* **66**, 830–842.

Jamison, W. R. 1987. Geometric analysis of fold development in overthrust terranes. *J. Struct. Geol.* **9**, 207–219

Jones, P. B. 1987. *Quantitative Geometry of Thrust and Fold Belt Structures. Methods in Exploration Series* **6** American Association of Petroleum Geologists, Tulsa, Oklahoma

Medwedeff, D. A. 1985. Lateral terminations of fault-related folds *Geol. Soc Am Abs. w. Prog.* **17**, 661

Medwedeff, D. A. In press. Geometry and kinematics of an active, laterally-propagating wedge thrust, Wheeler Ridge, California. In: *Structural Geology of Fold and Thrust Belts* (edited by Mitra, S. & Fisher, G.). John Hopkins University Press, Baltimore, Maryland

Mitra, S 1988 Geometry and evolution of the Pine Mountain thrust system, Appalachians. *Bull geol Soc. Am.* **100**, 72–95

Mitra, S. 1990 Fault-propagation folds· Geometry, kinematic evolution, and hydrocarbon traps. *Bull. Am Ass. Petrol Geol.* **74**, 921–945.

Rich, R. L 1934. Mechanics of low-angle overthrust faulting as illustrated by Cumberland thrust block, Virginia, Kentucky, and Tennessee. *Bull. Am. Ass. Petrol. Geol.* **18**, 1584–1596

Sanderson, D. J 1982. Models of strain variation in nappes and thrust sheets· a review. *Tectonophysics* **88**, 201–233.

Snedden, W. T & Spang, J. H. 1989. Geometric analysis of displace-

ment transfer between thrust faults using fault-bend and fault-propagation fold models *Geol Soc Am Abs w Prog* **21**, A67

Snedden, W T & Spang, J H. 1990 Geometric analysis of displacement transfer between thrust faults using fault-bend and fault-propagation fold models 1990 *Thrust Tectonics Conf Abs* 19

Suppe, J 1983. Geometry and kinematics of fault-bend folding *Am J Sci.* **283**, 648–721

Suppe, J 1985 *Principles of Structural Geology* Prentice-Hall, Englewood Cliffs, New Jersey

Suppe, J & Medwedeff, D A 1984 Fault-propagation folding *Geol Soc. Am Abs. w Prog* **16**, 670

Suppe, J & Medwedeff, D A In press Geometry and kinematics of fault-propagation folding *Eclog geol Helv* **83**

Wilkerson, M S 1989a *MacThrustRamp*! 1 0 Program and manual

Wilkerson, M S 1989b Three-dimensional computer modeling of fold-thrust structures *Geol Soc Am Abs w Prog* **21**, A63

Wilkerson, M S & Usdansky S I 1989 *MacFault*! 1 0 Program and manual

Wilkerson, M S 1990. Comparison of computer-generated, three-dimensional map patterns of similar and parallel folding algorithms in fold-thrust belts 1990 *Thrust Tectonics Conf. Abs.* 84

Woodward, N B , Boyer, S E & Suppe, J 1989 *Balanced Geological Cross-sections An Essential Technique in Geological Research and Exploration Short Course in Geology* **6**. American Geophysical Union, Washington, DC